A Generalized Procedure to Model Complex Time-Varying Physical Systems

Davide Tebaldi and Roberto Zanasi

***Abstract*— This letter addresses the systematic modeling of complex physical systems involving constant and time-varying interactions of physical elements in different energetic domains. The proposed procedure provides two different dynamic models of the considered system: a full-order one and a reduced-order one, where the latter is obtained when some of the system dynamical elements are properly disregarded. The matrices and vectors of the two dynamic models are automatically computed following the proposed rules and algorithms, thus reducing the chances of making computation mistakes. The proposed procedure is applied to two different case studies: an hydraulic continuous variable transmission for powertrain dynamics and a crank-connecting rod system in the mechatronic field.**

***Index terms*—** Modeling, Mechatronics, Time-varying systems, Model/Controller reduction.

I. INTRODUCTION

Modeling physical systems is a fundamental skill in any engineering field. With specific reference to the systems and control engineering field, a detailed and correct model of the physical systems under consideration allows to gain a deep understanding of their dynamic behavior, which is a very useful knowledge in order to develop new and effective control strategies to achieve the desired objectives.

The modeling of physical systems can be performed using many different approaches proposed in the literature at different levels of abstraction. In [1], the vehicle model is derived by directly writing down the kinematic and dynamic equations, whereas the power consumed by the vehicle is modeled in [2] as a function of vehicle velocity and control force. In [3], the powertrain model is performed by modeling the overall power demand to the fuel cell and to the battery. A strong simplification is instead made in [4] when modeling the vehicle gearbox, final drive and wheel radius as a single overall transmission ratio. The modeling of physical elements can also be performed using the different graphical formalisms available in the literature, that are Bond Graphs (BG) [5], Energetic Macroscopic Representation (EMR) [6] and Power-Oriented Graphs (POG) [7]-[10], offering differ pros and cons with respect to each other. An important aspect when modeling complex physical systems is the interaction between physical elements belonging to different energetic domains, including mechanical translational and rotational domains, hydraulic and electrical domains. A first instance is represented by a device called Continuous Variable Transmission (CVT), which is widely employed in power-split vehicle architectures and is composed of different physical elements depending on the considered CVT type. The Electro CVT (ECVT) [11]-[12] includes interactions between physical elements in the mechanical rotational and the electrical energetic domains, whereas the hydraulic CVT [11]-[12] includes interactions between physical elements in the mechanical rotational and the hydraulic energetic domains. Another instance of systems involving interactions between different energetic domains is represented by conveyor belts [13]-[14] and mechanical CVTs [11], [15], both involving the interaction between physical elements in the mechanical translational and rotational energetic domains. Many other instances of physical elements interactions between different energetic domains can be found in all engineering fields.

In [7]-[10], we proposed a systematic procedure for the fully automated modeling of many different devices which can be found in the transportation, mechatronic, robotics fields and many others. The considered devices include planetary gear sets [16]-[17], bevel gears [18]-[19], toroidal variators [20]-[21] which can be employed for applications such as Kinetic Energy Recovery System (KERS) and Infinitely Variable Trasmission (IVT), and vehicle differentials [22]-[23]. The procedure proposed in [7]-[10] offers the following important benefits with respect to other approaches in the literature: a) two state-space models of the system are automatically written using the proposed modeling rules: a full model accounting for the gears elastic coupling and a reduced model assuming rigid gears connection; b) the procedure to obtain the full and reduced models *is always the same* even in time-varying case; c) the matrices and vectors of the two system models can be systematically obtained using the proposed rules and algorithms; d) the reduced model is computationally efficient and can therefore be implemented in real-time; e) the reduced model can also provide the time behavior of the tangential forces that have been disregarded at the gears contact points.

In this letter, we would like to extend the procedure proposed in [7]-[10] by introducing the following new contributions: 1) the generalization of the proposed procedure in order to account for: 1.1) the presence of mechanical translational elements together with rotational elements; 1.2) gears (or masses, in this extended version) coupled not only by tangential springs, but also by other dynamical elements in other energetic domains (such as hydraulic accumulators, for example); 2) the generalization and simplification of Algorithm 1 proposed in [10]. The term *generalization* in 1) and 2) refers to the fact that the new Algorithm 1 proposed in this letter allows to automatically compute a

*This work was not supported by any organization

Davide Tebaldi and Roberto Zanasi are with the Department of Engineering "Enzo Ferrari", University of Modena and Reggio Emilia, Modena, Via Pietro Vivarelli 10 - int. 1 - 41125 Modena, Italy (e-mail: davide.tebaldi@unimore.it; roberto.zanasi@unimore.it).

generalized radii matrix accounting for systems including translational elements too, and to the fact that the system inertias and masses *can interact with each other through different dynamical elements belonging to different energetic domains*. The term simplification in 2) refers to the fact that the elements in the new generalized radii matrix are computed using a single sign function $S_{ij,h}$ resulting from a standard vectorial product, instead of two sign functions as it was in the previous work. This makes the procedure less prone to mistakes and lighter from a computational point of view. The new generalizations introduced in this letter allow to significantly extend the class of application of our systematic modeling procedure to many complex physical systems involving different physical elements interactions. In order to show the versatility of the proposed procedure, two new different case studies have been modeled using the proposed procedure: an hydraulic CVT, which includes gears coupled by elastic elements and by an hydraulic accumulator, and a Crank-Connecting Rod (CCR) system, which includes interactions between rotational and translational physical elements. With reference to the second case study, the comparison of our procedure with the typically employed Lagrangian approach is also addressed.

This letter is organized as follows. The systematic modeling and simulation of the hydraulic CVT case study are addressed in Sec. II and Sec. II-B, respectively. The new Algorithm 1 is in turn presented in Sec. II-A. The systematic modeling and simulation of the CCR case study are addressed in Sec. III and Sec. III-A, respectively, whereas the comparison with the Lagrangian approach is addressed in Sec. III-B. Finally, the conclusions are reported in Sec. IV.

II. Continuous Variable Transmission

Let us consider the hydraulic Continuous Variable Transmission system shown in Fig. 1. The CVT is a widely employed system in the automotive and agricultural fields; one of its main advantages is the introduction of a continuously-varying ratio decoupling the endothermic engine from the vehicle transmission system, thus allowing to optimize the endothermic engine fuel consumption. The hydraulic CVT system is composed of a planetary gear set and of a hydro-mechanical part, as highlighted in Fig. 1. The hydro-mechanical part is in turn composed of an hydraulic pump and an hydraulic motor charging and discharging an hydraulic accumulator, as shown in Fig. 2. The output volume flow rate $Q_p(\theta)$ of the hydraulic pump is function of the angular position θ of the pump plate. The pressure P_{de} within the hydraulic accumulator C_{de} is function of the hydraulic pump volume flow rate $Q_p(\theta)$ and of the hydraulic motor volume flow rate Q_m as follows: $C_{de}\dot{P}_{de} = Q_p(\theta) - Q_m$.

The hydraulic CVT can be modeled using the following dynamic model [10]:

$$\underbrace{\begin{bmatrix}\mathbf{J} & \mathbf{0}\\ \mathbf{0} & \mathbf{K}^{-1}\end{bmatrix}}_{\mathbf{L}}\dot{\mathbf{x}}=\underbrace{\begin{bmatrix}-\mathbf{B}_J-\mathbf{R}^{\mathrm{T}}(t)\mathbf{B}_K\mathbf{R}(t) & -\mathbf{R}^{\mathrm{T}}(t)\\ \mathbf{R}(t) & \mathbf{0}\end{bmatrix}}_{\mathbf{A}(t)}\mathbf{x}+\underbrace{\begin{bmatrix}\mathbf{I}\\ \mathbf{0}\end{bmatrix}}_{\mathbf{B}}\underbrace{\mathbf{u}}_{\boldsymbol{\tau}}, \tag{1}$$

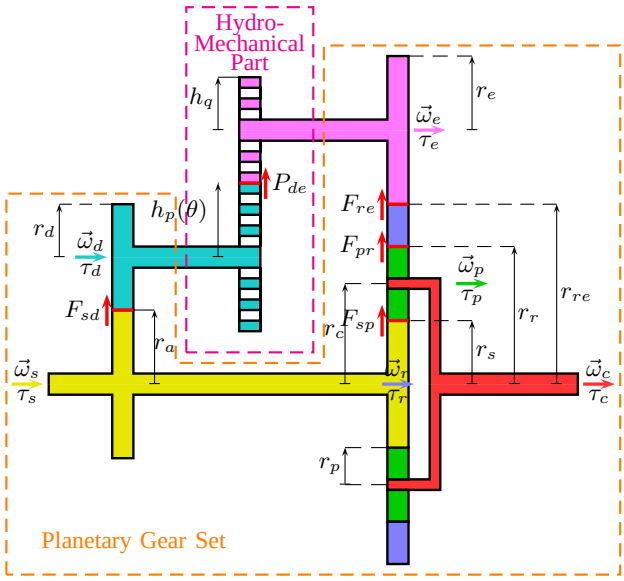

Fig. 1. Structure of the considered hydraulic CVT.

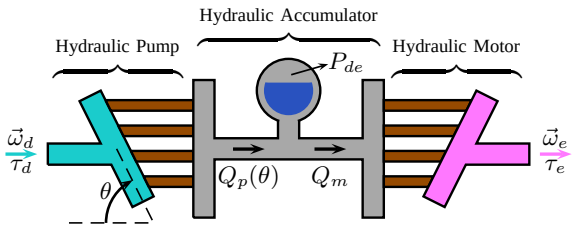

Fig. 2. Structure of the CVT hydraulic part.

where $\mathbf{x} = [\boldsymbol{\omega}^{\mathrm{T}} \ \mathbf{F}^{\mathrm{T}}]^{\mathrm{T}}$ and $\mathbf{u} = \boldsymbol{\tau}$ are the system state and input vectors, respectively, and $\mathbf{L}$, $\mathbf{A}(t)$ and $\mathbf{B}$ are the energy, power and input matrices, respectively. System (1) exhibits a one-to-one correspondence with the POG block scheme in Fig. 3, which can be directly implemented in the Simulink environment using very standard components. For the hydraulic CVT in Fig. 1, the set $\mathcal{N}_J$ containing the inertia and mass elements, the set $\mathcal{N}_K$ containing the coupling elements, and the set $\mathcal{N}_B$ containing the relative frictions acting between the system inertias [10] are defined as follows:

$$\begin{cases}\mathcal{N}_J = \{c,\ p,\ s,\ r,\ d,\ e\}, & n_J = \dim(\mathcal{N}_J) = 6,\\ \mathcal{N}_K = \{sp,\ pr,\ sd,\ re,\ de\}, & n_K = \dim(\mathcal{N}_K) = 5,\\ \mathcal{N}_B = \{\}, & n_B = \dim(\mathcal{N}_B) = 0.\end{cases} \tag{2}$$

Note that the last coupling element "de" in set $\mathcal{N}_K$ in (2) *is not elastic, but hydraulic instead*, and it describes the hydraulic capacitance C_{de} of the hydraulic accumulator in Fig. 2. From $\mathcal{N}_J$ in (2), the output speed vector $\mathbf{y} = \mathbf{B}^{\mathrm{T}}\mathbf{x} = \boldsymbol{\omega}$, the input torque vector $\mathbf{u} = \boldsymbol{\tau}$, the inertia matrix $\mathbf{J}$ and the gears friction matrix $\mathbf{B}_\omega$ are defined as:

$$\boldsymbol{\omega}=\begin{bmatrix}\omega_c\\ \omega_p\\ \omega_s\\ \omega_r\\ \omega_d\\ \omega_e\end{bmatrix}, \boldsymbol{\tau}=\begin{bmatrix}\tau_c\\ \tau_p\\ \tau_s\\ \tau_r\\ \tau_d\\ \tau_e\end{bmatrix}, \boldsymbol{J}=\begin{bmatrix}J_c & 0 & 0 & 0 & 0 & 0\\ 0 & J_p & 0 & 0 & 0 & 0\\ 0 & 0 & J_s & 0 & 0 & 0\\ 0 & 0 & 0 & J_r & 0 & 0\\ 0 & 0 & 0 & 0 & J_d & 0\\ 0 & 0 & 0 & 0 & 0 & J_e\end{bmatrix}, \boldsymbol{B}_\omega=\begin{bmatrix}b_c & 0 & 0 & 0 & 0 & 0\\ 0 & b_p & 0 & 0 & 0 & 0\\ 0 & 0 & b_s & 0 & 0 & 0\\ 0 & 0 & 0 & b_r & 0 & 0\\ 0 & 0 & 0 & 0 & b_d & 0\\ 0 & 0 & 0 & 0 & 0 & b_e\end{bmatrix}.$$

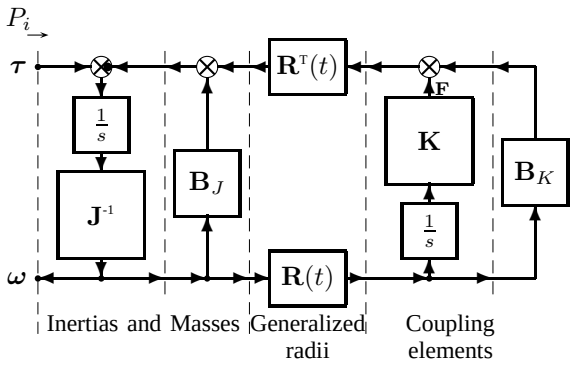

Fig. 3. POG scheme of time-varying physical systems.

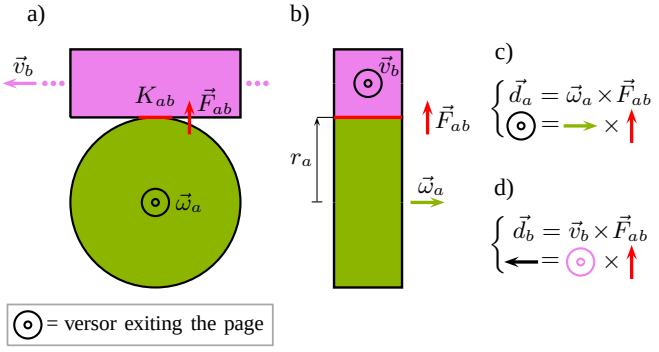

Fig. 4. Interaction between a rotational element "a" and a translational element "b" through an elastic coupling element K_{ab}.

From $\mathcal{N}_K$ in (2), the generalized force vector $\mathbf{F}$, stiffness matrix $\mathbf{K}$, and stiffness friction matrix $\mathbf{B}_K$ are defined as:

$$\mathbf{F}=\begin{bmatrix}F_{sp}\\F_{pr}\\F_{sd}\\F_{re}\\P_{de}\end{bmatrix}, \boldsymbol{K}=\begin{bmatrix}K_{sp}&0&0&0&0\\0&K_{pr}&0&0&0\\0&0&K_{sd}&0&0\\0&0&0&K_{re}&0\\0&0&0&0&C_{de}^{-1}\end{bmatrix}, \boldsymbol{B}_K=\begin{bmatrix}d_{sp}&0&0&0&0\\0&d_{pr}&0&0&0\\0&0&d_{sd}&0&0\\0&0&0&d_{re}&0\\0&0&0&0&R_{de}\end{bmatrix}.$$

The above vector and matrices are said to be *generalized* because they also contain the parameters of a coupling element which does not belong to the mechanical energetic domain: the hydraulic capacitance C_{de} of the hydraulic accumulator, the associated hydraulic resistance R_{de}, and the pressure P_{de} within the hydraulic accumulator. The relative friction matrix is $\mathbf{B}_{\Delta\omega}=\mathbf{0}$ according to set $\mathcal{N}_B$ in (2) and using Algorithm 2 in [10]. The inertia friction matrix is $\mathbf{B}_J=\mathbf{B}_\omega+\mathbf{B}_{\Delta\omega}=\mathbf{B}_\omega$. The generalized radii matrix $\mathbf{R}(t)$ can be automatically computed using the new Algorithm 1 described in Sec. II-A:

$$\begin{array}{c} \\ sp \\ pr \\ sd \\ re \\ de \end{array} \mathbf{R}(t)= \begin{array}{c} \begin{array}{cccccc} c & p & s & r & d & e \end{array} \\ \begin{bmatrix} -r_c & r_p & r_s & 0 & 0 & 0 \\ r_c & r_p & 0 & -r_r & 0 & 0 \\ 0 & 0 & r_a & 0 & r_d & 0 \\ 0 & 0 & 0 & r_{re} & 0 & r_e \\ 0 & 0 & 0 & 0 & h_p(\theta) & -h_q \end{bmatrix} \end{array}. \quad (3)$$

where $r_c = r_p + r_s$, $r_r = 2\,r_p + r_s$ and parameter $h_p(\theta) = K_p\theta$ is function of the time-varying angle θ of the hydraulic pump plate, see Fig. 2. Matrix $\mathbf{R}(t)$ in (3) is said to be *generalized* because it also contains the two parameters $h_p(\theta)$ and h_q which *are not gears radii*, and whose physical meaning is given in Remark 1 in Sec. II-A. When $\mathbf{K}\to\infty$ and when the hydraulic capacitance $C_{de}\to 0$, from the second equation in (1) one obtains $\mathbf{R}(t)\boldsymbol{\omega}=\mathbf{0}$. Using this last vectorial constraints, the n_J components of the speed vector $\boldsymbol{\omega}$ can be expressed as a function of $n_J - n_K = 1$ angular speeds composing the new state vector $\mathbf{x}_1$ of the reduced system: $\boldsymbol{\omega}=\mathbf{Q}_1(t)\mathbf{x}_1$. Choosing $\mathbf{x}_1=\omega_s$, one can write:

$$\underbrace{\begin{bmatrix}\boldsymbol{\omega}\\\mathbf{F}\end{bmatrix}}_{\mathbf{x}}=\underbrace{\begin{bmatrix}\mathbf{Q}_1(t)\\\mathbf{0}\end{bmatrix}}_{\mathbf{T}_1(t)}\underbrace{\mathbf{x}_1}_{\omega_s}, \quad \text{where} \quad \mathbf{Q}_1(t)=\begin{bmatrix}\frac{h_q r_d r_{re} r_s + K_p r_a r_e r_r \theta}{2 h_q r_d r_{re} r_c}\\ \frac{K_p r_a r_e r_r \theta - h_q r_d r_{re} r_s}{2 h_q r_d r_p r_{re}}\\ 1\\ \frac{K_p\, r_a\, r_e\, \theta}{h_q\, r_d\, r_{re}}\\ -\frac{r_a}{r_d}\\ -\frac{K_p\, r_a\, \theta}{h_q\, r_d}\end{bmatrix},$$

where $\mathbf{x}=\mathbf{T}_1(t)\mathbf{x}_1$ is a time-varying congruent transformation relating the original state vector $\mathbf{x}$ of the full system (1) to the chosen new state vector $\mathbf{x}_1=\omega_s$ of the reduced system. By applying $\mathbf{x}=\mathbf{T}_1(t)\mathbf{x}_1$ to system (1), one obtains the following reduced state space time-varying model:

$$\mathbf{L}_1(t)\,\dot{\mathbf{x}}_1+\mathbf{N}_1(t)\,\mathbf{x}_1=\mathbf{A}_1(t)\,\mathbf{x}_1+\mathbf{B}_1(t)\,\boldsymbol{\tau}, \quad (4)$$

where $\mathbf{L}_1(t)=\mathbf{Q}_1(t)^{\mathrm{T}}\mathbf{J}\,\mathbf{Q}_1(t)$, $\mathbf{N}_1(t)=\mathbf{Q}_1(t)^{\mathrm{T}}\mathbf{J}\,\dot{\mathbf{Q}}_1(t)$, $\mathbf{A}_1(t)=-\mathbf{Q}_1(t)^{\mathrm{T}}\mathbf{B}_J\mathbf{Q}_1(t)$ and $\mathbf{B}_1(t)=\mathbf{Q}_1^{\mathrm{T}}(t)$.

A. Algorithm 1: the Generalized Radii Matrix $\mathbf{R}(t)$

Let $r_{ij,h}(t)$ denote the generic coefficient of matrix $\mathbf{R}(t)=[r_{ij,h}(t)]$, where $ij\in\mathcal{N}_K$ and $h\in\mathcal{N}_J$, see (2).

Property 1: The generic coefficient $r_{ij,h}(t)$ of the generalized radii matrix $\mathbf{R}(t)$ can be computed as follows:

$$r_{ij,h}(t)=S_{ij,h}\,r_h(t). \quad (5)$$

The definition of parameters $S_{ij,h}$ and r_h differs depending on the type of the considered physical element h:

- *Inertia (rotational) element*: in this case, the effective radius r_h is the distance between the rotation axis of the inertia element h and the coupling element ij, whereas $S_{ij,h}$ is a sign term computed as follows:

$$S_{ij,h}=\begin{cases}1 & \text{if } \vec{d}_h=\vec{\omega}_h\times\vec{F}_{ij} \text{ is exiting the page,}\\ -1 & \text{if } \vec{d}_h=\vec{\omega}_h\times\vec{F}_{ij} \text{ is entering the page,}\end{cases}$$

where $\vec{\omega}_h$ and $\vec{F}_{ij}$ are vectors identifying the positive directions of the angular speed ω_h and of the generalized force F_{ij} of the coupling element ij. Fig. 4a shows an example involving a rotational element a interacting with a translational element b through an elastic element K_{ab}. Eq. 5 can be used with reference to Fig. 4b, showing the same physical system as Fig. 4a with a view rotated by

$\pi/2$. In this example, it is $r_h = r_a$ and $S_{ab,a} = 1$ since $\vec{d}_a = \vec{\omega}_a \times \vec{F}_{ab}$ *is exiting the page* by applying the right-hand rule, see Fig. 4c.

Note: in the CVT of Fig 1, element c affects the coupling elements pr and sp through an intermediate gear p. In this case, the effective radius is the distance between the rotation axes of the two angular speeds $\vec{\omega}_c$ and $\vec{\omega}_p$ [10], namely r_c.

• *Mass (translational) element*: in this case, the effective radius r_h is always equal to 1, whereas $S_{ij,h}$ is a sign term computed as follows:

$$S_{ij,h} = \begin{cases} 1 \text{ if } \vec{d}_h = \vec{v}_h \times \vec{F}_{ij} \text{ points toward the left of } \vec{F}_{ij}, \\ -1 \text{ if } \vec{d}_h = \vec{v}_h \times \vec{F}_{ij} \text{ points toward the right of } \vec{F}_{ij}, \end{cases}$$

where $\vec{v}_h$ is a vector identifying the positive direction of the translational speed v_h and where the left and right sides of $\vec{F}_{ij}$ are determined moving along the positive direction of vector $\vec{F}_{ij}$, see the red arrows in Fig. 4. With reference to the example in Fig. 4b, it is $r_h = r_b = 1$ and $S_{ab,b} = 1$, since $\vec{d}_b = \vec{v}_b \times \vec{F}_{ab}$ *points towards the left of* $\vec{F}_{ab}$ by applying the right-hand rule, see Fig. 4d.

Therefore, the generalized radii matrix $\mathbf{R}$ of the example shown in Fig. 4 is:

$$_{ab}\mathbf{R} = \begin{bmatrix} \overset{a}{r_a} & \overset{b}{1} \end{bmatrix}.$$

Remark 1: When the rotational element h is connected to a physical element from a different energetic domain, the *generalized* effective radius r_h handles the energy conversion between the two different energetic domains.

Example: in the CVT of Fig. 1 and Fig. 2, the rotational elements d and e interact with the hydraulic pump and the hydraulic motor through the generalized affective radii $h_p(\theta)$ and h_q, respectively. $h_p(\theta)$ and h_q are the coefficients that, multiplied by the angular speeds ω_d and ω_e, give the volume flow rates $Q_p(\theta)$ and Q_m entering and exiting the hydraulic accumulator C_{de}, respectively.

B. Simulations

The full and reduced models (1) and (4) of the considered hydraulic CVT shown in Fig. 1 have been simulated using the inputs, initial conditions and parameters reported in Table I. The obtained simulation results are shown in Fig. 5. In particular, the time behaviors of the angular speeds ω_i, for $i \in \mathcal{N}_J$ in (2), are shown in the left subplot of Fig. 5, whereas the time behaviors of the tangential forces F_{ij} and of the pressure P_{de}, for $ij \in \mathcal{N}_K$ in (2), are shown in the middle and in the right subplot, respectively. The continuous colored plots refer to the simulation results given by the full model (1). The red dashed plots of the angular speeds ω_i on the left subplot of Fig. 5 are obtained using the reduced model (4), whereas the red dashed plots of the tangential forces F_{ij} in the middle subplot of Fig. 5 and the red dashed plot of the pressure P_{de} in the right subplot have been obtained using [10]-Eq. (11). This proves that the latter equation, which is one of the contributions of our previous work, works to provide the power variables of all coupling dynamic elements that are no longer present in the reduced model (i.e., not only the tangential forces, as it was instead in the previous work, but also the power variables of the other coupling elements too, e.g. the pressure P_{de} within the hydraulic accumulator C_{de} in the considered case study.). Fig. 5 shows the very good matching between the simulation results obtained using the full and reduced models. The middle subplot of the figure shows the fast oscillations that some tangential forces F_{ij} exhibit, that are due to the high value of the stiffness coefficients K_{ij} in Table I. The full model is indeed more suitable for accurate simulations, in order to know the exact behavior of the coupling dynamic elements present in matrix $\mathbf{K}$. The reduced model is instead very suitable for developing real-time control strategies for the considered system. This is thanks to the fact that fixed-step simulations can be better performed with the reduced model, because the fast dynamics of the coupling elements in matrix $\mathbf{K}$ is not present any longer.

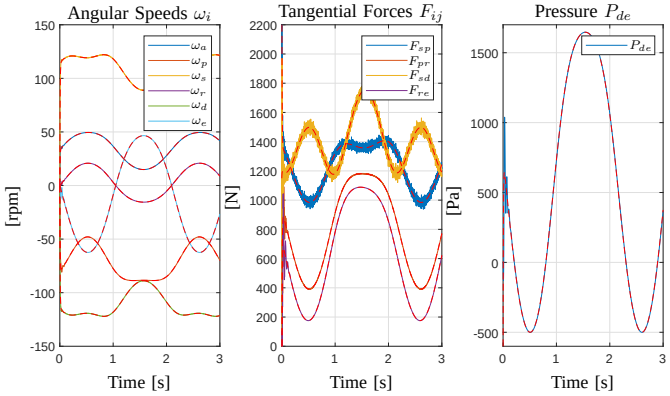

Fig. 5. Simulation of the Hydraulic CVT: full model (colored characteristics) and reduced model (dashed characteristics).

TABLE I

HYDRAULIC CVT: SIMULATION PARAMETERS.

$r_r = 24.8$ cm, $J_r = 2.18$ kg m^2, $r_c = 17.5$ cm, $J_c = 0.929$ kg m^2
$r_p = 7.3$ cm, $J_p = 0.081$ kg m^2, $r_d = 10$ cm, $J_d = 0.05$ kg m^2
$r_e = 10$ cm, $J_e = 0.05$ kg m^2, $r_s = 10.2$ cm, $J_s = 0.049$ kg m^2
$r_{re} = 30$ cm, $r_a = 10$ cm, $K_p = 10$ l/rpm, $\theta = 30 \sin(3t)$, $h_q = K_p$
$b_c = b_p = b_s = b_r = 20$ Nm sec/rad, $b_d = b_e = 10$ Nm sec/rad
$K_{sp} = K_{pr} = K_{sd} = K_{re} = 10^8$ N/m, $C_{de} = 1\mu$Pa$/m^3$
$d_{sp} = d_{pr} = d_{sd} = d_{re} = 10$ N sec/m, $R_{de} = 0$
$\boldsymbol{\tau} = [0\ 0\ 500\ 0\ 0\ 0]^{\mathrm{T}}$ Nm, $\boldsymbol{\omega}_0 = [0\ 0\ 0\ 0\ 0\ 0]^{\mathrm{T}}$, $\mathbf{F}_0 = [0\ 0\ 0\ 0\ 0]^{\mathrm{T}}$

III. CRANK-CONNECTING ROD

Let us consider the Crank-Connecting Rod (CCR) system shown in Fig. 6a. From the modeling point of view, this system can be considered as a special case of the system composed of a translational element and a rotational element interacting with each other shown in Fig. 4, in which radius r_a is now function of the time-varying angle θ: $r_a = r_a(\theta)$, see Fig. 6a. In order to apply the proposed systematic modeling procedure as described in Property 1 in Sec. II-A, reference has to be made to the schematic representation of the CCR system shown in Fig. 6b. This system can be modeled using the same full dynamic model (1). The sets $\mathcal{N}_J$, $\mathcal{N}_K$ and $\mathcal{N}_B$ are:

$$\begin{cases} \mathcal{N}_J = \{a, b\}, & n_J = \dim(\mathcal{N}_J) = 2, \\ \mathcal{N}_K = \{ab\}, & n_K = \dim(\mathcal{N}_K) = 1, \\ \mathcal{N}_B = \{\}, & n_B = \dim(\mathcal{N}_B) = 0. \end{cases} \quad (6)$$

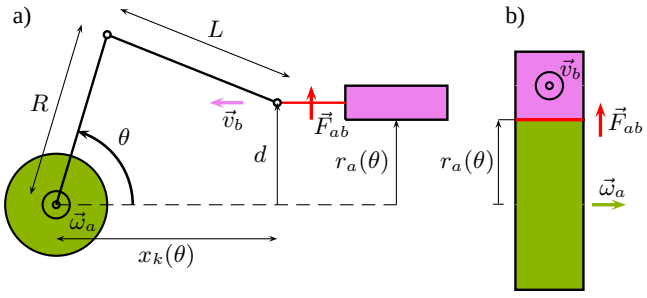

Fig. 6. Structure of the considered Crack-Connecting Rod system.

From $\mathcal{N}_J$ and $\mathcal{N}_K$ in (6), the output speed vector $\mathbf{y} = \mathbf{B}^{\mathrm{T}}\mathbf{x} = \boldsymbol{\omega}$, the input torque vector $\mathbf{u} = \boldsymbol{\tau}$, the inertia matrix $\mathbf{J}$, the gears friction matrix $\mathbf{B}_\omega$, the force vector $\mathbf{F}$, the stiffness matrix $\mathbf{K}$ and the stiffness friction matrix $\mathbf{B}_K$ result to be:

$$\boldsymbol{\omega}=\begin{bmatrix}\omega_a\\ v_b\end{bmatrix}, \boldsymbol{\tau}=\begin{bmatrix}\tau_a\\ F_b\end{bmatrix}, \boldsymbol{J}=\begin{bmatrix}J_a & 0\\ 0 & M_b\end{bmatrix}, \boldsymbol{B}_\omega=\begin{bmatrix}b_a & 0\\ 0 & b_b\end{bmatrix}, \quad \begin{matrix}\mathbf{F}=F_{ab},\\ \mathbf{K}=K_{ab},\\ \mathbf{B}_K=d_{ab}.\end{matrix}$$

Even in this case, the relative friction matrix is $\mathbf{B}_{\Delta\omega}=\mathbf{0}$ and the inertia friction matrix is $\mathbf{B}_J = \mathbf{B}_\omega$. Note that vectors $\boldsymbol{\omega}$, $\boldsymbol{\tau}$ and matrices $\mathbf{J}$, $\mathbf{B}_\omega$ assume a generalized meaning in this case, since they also include the parameters of the translational element b: the translational speed v_b, the input force F_b, the mass M_b and the friction coefficient b_b. The generalized radii matrix $\mathbf{R}(t)$ can be directly computed using the Algorithm 1 presented in Sec. II-A:

$$\overset{ab}{\mathbf{R}}(t) = \begin{bmatrix} \overset{a}{r_a(\theta)} & \overset{b}{1} \end{bmatrix}. \tag{7}$$

In this case, the generalized radius $r_a(\theta)$ is the coefficient that, multiplied by the angular speed ω_a, provides the tangential speed $v_a = r_a(\theta)\omega_a$ at first terminal of the elastic element K_{ab}. Coefficient $r_a(\theta)$ is function of the time-varying angle θ representing the angular position of the rotational element a in Fig. 6, and can be expressed as follows:

$$H(\theta)=\frac{\partial x_k(\theta)}{\partial\theta} = R\left[-\sin\theta - \frac{(\sin\theta-\beta)\cos\theta}{\sqrt{\alpha^2-(\sin\theta-\beta)^2}}\right],$$

where $\alpha = L/R > 1$, $\beta = d/R < 1$ and $\omega_a = \frac{d\theta}{dt}$. When $\mathbf{K} = K_{ab} \to \infty$, from the second equation in (1) one obtains $\mathbf{R}(t)\boldsymbol{\omega} = \mathbf{0}$, which can be used to express the original state vector $\mathbf{x}$ as a function of the chosen reduced state vector $\mathbf{x}_1 = \omega_a$ as follows:

$$\underbrace{\begin{bmatrix}\boldsymbol{\omega}\\ \mathbf{F}\end{bmatrix}}_{\mathbf{x}} = \underbrace{\begin{bmatrix}\mathbf{Q}_1(t)\\ \mathbf{0}\end{bmatrix}}_{\mathbf{T}_1(t)} \underbrace{\mathbf{x}_1}_{\omega_a} \quad \text{where} \quad \mathbf{Q}_1(t)=\begin{bmatrix}1\\ -r_a(\theta)\end{bmatrix} \tag{8}$$

and where the time-varying congruent transformation $\mathbf{x} = \mathbf{T}_1(t)\mathbf{x}_1$ applied to system (1) gives *the same* reduced model (4) obtained for the CVT case study.

A. Simulations

This section deals with the simulation of the full and reduced models (1) and (4) of the considered Crank-Connecting Rod system shown in Fig. 6. The two simulations

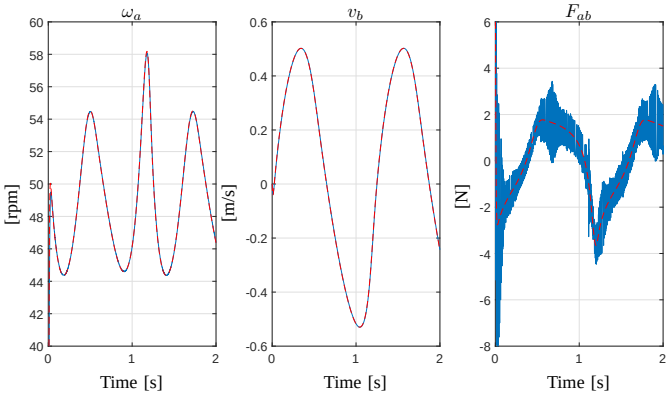

Fig. 7. Simulation of the CCR: full model (light blue characteristics) and reduced model (dashed characteristics).

TABLE II

CCR: SIMULATION PARAMETERS.

$R=10$ cm, $L=40$ cm, $d=5$ cm, $J_a=0.0013$ kg m^2, $M_b=0.8$ Kg
$K_{ab}=10^8$ N/m, $b_a=0.191$ Nm sec/rad, $b_b=0.5$ Nm sec/m
$d_{ab}=10$ Nm sec/m, $\boldsymbol{\tau}=\begin{bmatrix}1 & 0\end{bmatrix}^{\mathrm{T}}$ Nm, $\boldsymbol{\omega}_0=\begin{bmatrix}0 & 0\end{bmatrix}^{\mathrm{T}}$, $\mathbf{F}_0=0$

have been performed using the inputs, initial conditions and parameters reported in Table II. The results in terms of angular speed ω_a, translational speed v_b and tangential force F_{ab} are shown in Fig. 7: the light blue characteristics refer to the simulation performed using the full model (1) and the red dashed characteristics refer to the simulation performed using the reduced model (4). The time behavior of the tangential force F_{ab} in the reduced model case has been obtained using [10]-Eq. (11). Similar comments as those made in Sec. II-B on Fig. 5 regarding the simulation of the hydraulic CVT can be made in this case as well. In particular, from Fig. 7 it is possible to observe the very good matching between the results given by the full model, which is suitable for detailed simulations, and the reduced model, which is suitable for developing real-time control strategies.

B. Comparison with the Lagrangian Approach

The CCR could have been modeled using other approaches too, such as the following Lagrange Equations:

$$\frac{d}{dt}\left(\frac{\partial T}{\partial \dot{q}_i}\right) - \frac{\partial T}{\partial q_i} + \frac{\partial U}{\partial q_i} = Q_i \qquad i = 1, \ldots, N, \tag{9}$$

where N is the number of degrees of freedom in the system, q_i and Q_i are the generalized Lagrangian coordinates and forces, T and U are the kinetic and potential energies in the system. By applying (9) to the CCR system, it results:

$$\begin{aligned} &T = \tfrac{1}{2}J_a\omega_a^2 + \tfrac{1}{2}M_b v_b^2 \qquad U = 0, \qquad q_1 = \theta,\\ &Q_1 = \tau_a - b_a\omega_a - b_b\, r_a(\theta)^2\omega_a + r_a(\theta)\, F_b. \end{aligned} \tag{10}$$

One can verify that the model obtained applying (9)-(10) coincides with the reduced model (4) of the CCR system. However, the procedure we propose in this letter exhibits the following important features over the Lagrangian approach: a) The procedure is always the same for *any physical system* including inertia and mass elements, which can be coupled by elements that *may also not belong to the mechanical domain*, e.g. hydraulic accumulators etc. This means that our procedure allows to model a *larger class of systems* and in

an *automatic way*, and is therefore less subject to mistakes with respect to the Lagrangian approach. b) The Lagrangian approach requires the exact manual computation of the kinetic energy T, the potential energy U and the generalized force terms Q_i in (9). These terms can become very complex to compute especially if the number and the types of frictions (e.g. relative frictions) and the number of inertia and mass elements in the system increase. The level of complexity further increases if one wants to compute the full model (1) including the elastic interactions using the Lagrangian approach. Using our systematic procedure, all these computations are automatically given, see (8). Furthermore, the distinction between motive and friction torques and forces is automatic using the proposed systematic procedure, as the signs of the terms Q_i in (9) are automatically determined in the matrices $\mathbf{A}_1(t)$ and $\mathbf{B}_1(t)$ of the reduced model (4). c) If one wanted to find both the full model and the reduced model using the Lagrangian approach, the Lagrangian equations (9) should be applied twice. On the other hand, the proposed systematic modeling procedure directly gives the two models at the same time: the full model describing the effect of the coupling elements (elasticities, hydraulic accumulators, etc) on the system inertias and masses in details, and the reduced model being suitable for developing real-time control strategies for the considered system. Furthermore, using the proposed procedure, the output power variables of the coupling elements can still be computed in the reduced model using [10]-Eq. 10. d) On the contrary with respect to the Lagrangian approach, the procedure proposed in this letter allows to significantly extend the class of physical systems that can be modeled using it, including many complex physical systems involving physical interactions *in different energetic domains* other than the mechanical one.

IV. Conclusions

This letter has addressed the systematic modeling of complex physical systems involving different energetic domains. The proposed procedure directly provides the full and reduced models of the system; furthermore, the proposed rules and algorithms automatically provide all the system matrices and vectors. The two obtained models are derived automatically, thus reducing the risk of making computational mistakes for the user. The two provided system models have a different degree of detail: the full model is suitable for detailed simulations, whereas the reduced model is suitable for developing real-time control strategies. The proposed modeling procedure has been applied to two different case studies: an hydraulic continuous variable transmission for powertrain dynamics and a crank-connecting rod system in the mechatronic field. The considered case studies and the description of the proposed modeling procedure show the versatility of the procedure itself.

References

[1] Y. Wang, N. Bian, L. Zhang, H. Chen, "Coordinated lateral and longitudinal vehicle-following control of connected and automated vehicles considering nonlinear dynamics", *IEEE Contr. Syst. Lett.*, vol. 4, no. 4, pp. 1054-1059, Oct. 2020.

[2] G. P. Padilla, S. Weiland, M. C. F. Donkers, "A global optimal solution to the eco-driving problem", *IEEE Contr. Syst. Lett.*, vol. 2, no. 4, pp. 599-604, Oct. 2018.

[3] K. Choi, W. Kim, "Real-time predictive energy management strategy for fuel cell-powered unmanned aerial vehicles based on the control-oriented battery model", *IEEE Contr. Syst. Lett.*, vol. 7, pp. 943-948, Dec. 2022.

[4] D. Shen, D. Karbowski, A. Rousseau, "Solving eco-driving problems using indirect collocation method and smooth representation", *IEEE Contr. Syst. Lett.*, vol. 5, no. 5, pp. 1501-1506, Nov. 2021.

[5] J. Velazquez Alcantar, F. Assadian, "Longitudinal tire force estimation using youla controller output observer", *IEEE Contr. Syst. Lett.*, vol. 2, no. 1, pp. 31-36, Jan. 2018.

[6] B.-H. Nguyen, R. German, J. P. F. Trovão, A. Bouscayrol, "Real-time energy management of battery/supercapacitor electric vehicles based on an adaptation of pontryagin's minimum principle", *IEEE Trans. Veh. Technol.*, vol. 68, no. 1, pp. 203-212, Jan. 2019.

[7] R. Zanasi, D. Tebaldi, "Planetary gear modeling using the power-oriented graphs technique", *IEEE European Control Conference*, Naples, Italy, Jun. 25-28, 2019.

[8] R. Zanasi, D. Tebaldi, "Power-oriented modeling of epicyclic gear trains", *IEEE Vehicle Power and Propulsion Conference*, Gijon, Spain, Nov. 18-Dec. 16, 2020.

[9] R. Zanasi, D. Tebaldi, "Modeling of complex planetary gear sets using power-oriented graphs", *IEEE Trans. Veh. Technol.*, vol. 69, no. 12, pp. 14470-14483, Dec. 2020.

[10] D. Tebaldi, R. Zanasi, "Systematic modeling of complex time-variant gear systems using a power-oriented approach", *Control Engineering Practice*, vol. 132, Mar. 2023.

[11] J. M. Miller, "Hybrid electric vehicle propulsion system architectures of the e-CVT type", *IEEE Trans. Power Electron.*, vol. 21, no. 3, pp. 756-767, May 2006.

[12] J. M. Miller, M. Everett, "An assessment of ultra-capacitors as the power cache in toyota THS-11, GM-allision AHS-2 and ford FHS hybrid propulsion systems", *Twentieth Annual IEEE Applied Power Electronics Conference and Exposition, 2005. APEC 2005.*, Austin, TX, USA, Mar. 06-10, 2005.

[13] G.-N. Zhu, Y. Zeng, S. Teoh, E. Toh, C. Y. Wong, I. M. Chen, "A bin-picking benchmark for systematic evaluation of robotic-assisted food handling for line production", *IEEE/ASME Trans. Mechatronics*, Early Access, Dec. 2022.

[14] S. Dey, O. Salim, H. Masoumi, N. C. Karmakar, "A novel UHF RFID sensor based crack detection technique for coal mining conveyor belt", *IEEE J. Radio Freq. Identificat.*, vol. 6, pp. 19-30, 2022.

[15] P. Setlur, J. R. Wagner, D. M. Dawson, B. Samuels, "Nonlinear control of a continuously variable transmission (CVT)", *IEEE Trans. Control Syst. Technol.*, vol. 11, no. 1, pp. 101-108, Jan. 2003.

[16] H. Hou, H. Ji, "Improved multiclass support vector data description for planetary gearbox fault diagnosis", *Control Engineering Practice*, vol. 114, Sep. 2021.

[17] A. Khajepour, M. S. Fallah, A. Goodarzi, "Electric and hybrid vehicles: technologies, modeling and control - a mechatronic approach", *John Wiley & Sons*, 2014.

[18] J. Du, J. Mao, Y. Cui, K. Liu, G. Zhao, "Theoretical and experimental study on load sharing of a novel power split spiral bevel gear transmission", *Adv. Mech. Eng.*, vol. 10, no. 6, pp. 1-9, 2018.

[19] W. G. Molyneux, "The internal bevel gear and its applications", *Proc. Inst. Mech. Eng. Part G: J. Aerosp. Eng.*, vol. 211, no. 1, pp. 39-61, 1997.

[20] R. Fuchs, Y. Hasuda, I. James, "Full toroidal IVT variator dynamics", *SAE Technical Paper 2002-01-0586*, 2002.

[21] J. P. Newall, S. Cowperthwaite, M. Hough, A. P. Lee, "Efficiency modelling in the full toroidal variator: investigation into optimisation of EHL contact conditions to maximize contact efficiency", *Tribol. Interface Eng. Ser.*, vol. 48, pp. 245-255, 2005.

[22] M. Forstinger, R. Bauer, A. Hofer, W. Rossegger, "Multivariable control of a test bed for differential gears", *Control Engineering Practice*, vol. 57, pp. 18-28, Dec. 2016.

[23] M. Gadola, D. Chindamo, "The mechanical limited-slip differential revisited: high-performance and racing car applications", *Int. Journal of Applied Engineering Research*, vol. 13, no. 2, pp. 1478-1495, 2018.